Matter and Radiation at Extremes

REVIEW ARTICLE

scitation.org/journal/mre

Research at Tsinghua University on electrical explosions of wires

Cite as: Matter Radiat. Extremes 4, 017201 (2019); doi: 10.1063/1.5081450
Submitted: 26 June 2018 • Accepted: 24 September 2018 •
Published Online: 17 January 2019

Xinxin Wang[a)]

AFFILIATIONS

Department of Electrical Engineering, Tsinghua University, Beijing 100084, China

[a)]Author to whom correspondence should be addressed: wangxx@tsinghua.edu.cn

ABSTRACT

Electrical explosion of a wire (EEW) has been investigated for more than ten years at Tsinghua University, and the main results are reviewed in this paper. Based on EEW in vacuum, an X-pinch was used as an x-ray source for phase-contrast imaging of small insects such as mosquitoes and ants in which it was possible to observe clearly their detailed internal structures, which can never be seen with conventional x-ray radiography. Electrical explosion of a wire array (EEWA) in vacuum is the initial stage in the formation of a wire-array Z-pinch. The evolution of EEWA was observed with x-ray backlighting using two X-pinches as x-ray sources. It was found that each wire in an EEWA exhibits a core–corona structure instead of forming a fully vaporized metallic vapor. This structure is detrimental to the plasma implosion of a Z-pinch. By inserting an insulator as a flashover switch into the cathode, formation of a core–corona structure was suppressed and core-free EEWA was realized. EEW in gases was used for nanopowder production. Three parameters (vaporization rate, gas pressure, and energy deposited in the exploding plasma) were found to influence the nanoparticle size. EEW in water was used for shock-wave generation. The shock wave generated by melting could be recorded with a piezoelectric gauge only in underheat EEW. For EEW with a given stored energy but different energy-storage capacitor banks, the small capacitor bank produced a rapidly rising current that deposited more energy into the wire and generated a stronger shock wave.

I. INTRODUCTION

Electrical explosion of a wire (EEW) is performed by passing a pulsed high current through a metallic wire.[1] As the energy deposited in the wire by Joule heating increases, the wire undergoes rapid phase transitions (solid → liquid → vapor → plasma) as a result of the increase in its temperature. If the energy deposition is very fast and the deposited energy E_d is higher than that required for vaporization, i.e., $E_d > E_v$, then the wire may start to vaporize. This is called the "overheat" phenomenon. When the wire starts to vaporize, its electrical resistance dramatically rises, and one of three discharge modes—cutoff current, restrike, or breakdown—occurs, depending on the wire voltage and the density of the expanding metallic vapor from the vaporizing wire. The waveforms of the currents for these three different discharge modes are shown in Fig. 1. The essential difference among these three discharge modes is the time delay between the first current pulse and the second current pulse that results from secondary breakdown in the metallic vapor from the vaporizing wire. If secondary breakdown does not occur, which could be considered as an infinitely long time delay of the breakdown, this is the "cutoff current" mode. If secondary breakdown occurs after the first current pulse has fully cut off, this is the "restrike" mode. If secondary breakdown occurs before the first current pulse has fully cut off, this is the "breakdown" mode.

EEW can be conducted in a variety of surrounding media (vacuum, gas, liquid, or solid) and behaves differently in each case, allowing different applications. In this paper, we present experimental results on EEW obtained at Tsinghua University, including EEW in vacuum for X- and Z-pinches, in gases for nanopowder production, and in liquids for the generation of shock waves.

II. EEW IN VACUUM FOR X- AND Z-PINCHES

A. EEW in vacuum for an X-pinch

For use as the load of a pulsed power generator, an X-pinch is formed in vacuum from two fine wires in the form of an "X" and touching at a single point. As a result of compression by the

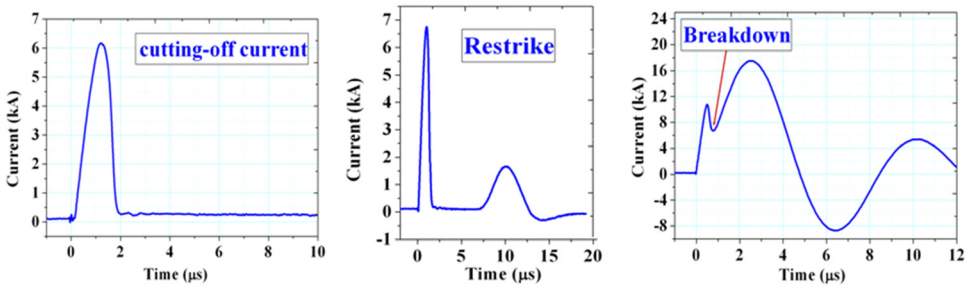

FIG. 1. Current waveforms for the three discharge modes.

magnetic field generated by the current in the wires, the plasma at the point of contact forms an extremely hot and dense point (X-pinch) that emits intense pulsed x-rays.[2] Such an X-pinch is sketched in Fig. 2.

Figure 3 shows a typical image of the x-ray point source and a typical waveform of the x-ray pulse from an X-pinch. It has been found that an X-pinch is an ideal x-ray point source for radiography with a temporal resolution of less than a nanosecond and a spatial resolution in the micrometer range.

The X-pinch device used in our laboratory is a compact and portable device, PPG-2, with five components: a Marx generator, a pulse forming line (PFL), a V/N switch, a pulse transmission line (PTL), and an X-pinch load. The Marx generator consists of six 0.15-μF capacitors charged in parallel to a maximum voltage of 60 kV and then discharged in series to the PFL. The PFL uses deionized water as insulating dielectric and is 1 m long, forming a 60 ns pulse. The characteristic impedance of the PFL is 1.25 Ω. The parameters of the PTL are the same as those of the PFL, except that its length is only 0.3 m for the sake of compactness. PPG-2 is capable of delivering to the X-pinch load a current of amplitude 100 kA and pulse width 60 ns.

There are two kinds of x-ray radiography: conventional radiography and phase-contrast radiography (PCR). While conventional radiography relies on x-ray absorption as the sole source of contrast, PCR uses phase variations as an additional source of contrast by recording the interference between x-rays passing through neighboring parts of the sample.[3,4] PCR offers improved contrast when imaging weakly x-ray-absorbing samples and has biological and clinical applications.

Since PCR is based on the interference of x-rays, it requires from the x-ray source a long spatial coherence length that is proportional to the ratio d/σ, where d is the distance from the source to the observation point and σ is the source size. Thus, high spatial coherence may be achieved by using a source of small size or by observing the beam at a large distance from the source. The intense and small x-ray source makes an X-pinch perfect for PCR. We used such an X-pinch x-ray source and took PCR images of small insects such as ants and mosquitoes.[5]

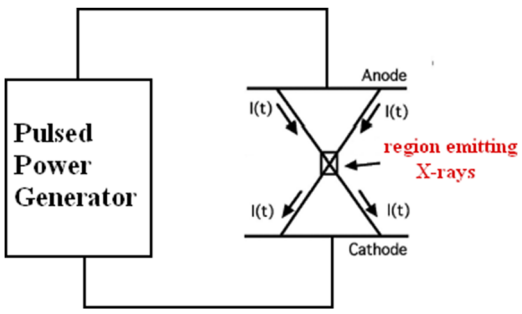

FIG. 2. Sketch of an X-pinch.

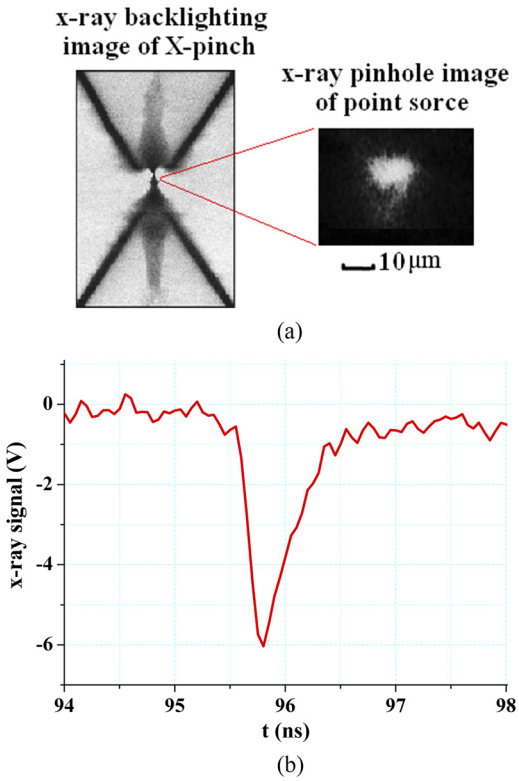

FIG. 3. (a) Typical image of x-ray point source and (b) waveform of an x-ray pulse from an X-pinch.

Figure 4 is a PCR image of a 3-mm-long ant in which we can see clearly details inside the ant's body that are never visible with conventional x-ray radiography.

Based on our experimental results, the X-pinch has proved to be an ideal x-ray source for PCR of weakly x-ray-absorbing samples, which makes it promising for clinical and biological applications. For example, in mammography, there is a need to distinguish between different kinds of soft tissue, namely, tumors and normal tissue. Because absorption in such cases is small, and the differences in density and composition between the different tissues are slight, conventional x-ray radiography is not very successful at this task.

FIG. 4. PCR image of a 3-mm-long ant.

B. EEW in vacuum for a wire-array Z-pinch

A wire-array Z-pinch is constructed by using a cylindrical array of wires in vacuum as the discharge load. The wire array is several centimeters in diameter and made of hundreds of fine wires. Figure 5 shows the physical processes involved in the formation of a wire-array Z-pinch.[6]

When a pulsed high current flows through a wire array, all the wires are electrically exploded into a cylindrical plasma shell in a process called electrical explosion of a wire array (EEWA). Under compression by the magnetic field generated by the current flowing through the plasma shell, plasma implosion occurs. As the radius of the plasma shell becomes smaller and smaller owing to the implosion, the plasma density and temperature become higher and higher. When the magnetic compressive force is balanced by the thermal pressure inside the compressed plasma shell, the plasma stagnates near the axis of the plasma shell, and intensive pulsed x-rays are emitted by the extremely hot pinched plasma.

In 1997, a breakthrough was made in Z-pinch research at Sandia Laboratories,[7] apparently due, at least in part, to the use

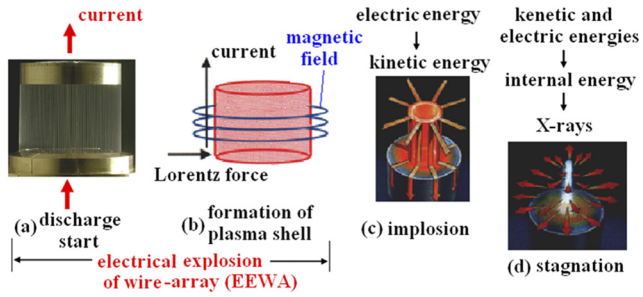

FIG. 5. Physical process involved in the formation of a wire-array Z-pinch.

of a wire array as the Z-pinch load. It was believed that there exists an ideal EEWA in which all the wires are simultaneously and completely exploded into plasma, which then merges into a uniform and cylindrically symmetric plasma shell. This ideal EEWA lowers the seed level for plasma instability and thus leads to a perfect plasma implosion. However, by taking backlighting images of EEWA using X-pinches as the x-ray sources, we found that the real EEW is very different from the idealized one.[8]

The experiment was performed on a pulsed power generator, PPG-1, capable of delivering to the load a 400 kA current in 100 ns.[9] PPG-1 has five components: a Marx generator, a PFL, a V/N switch, a PTL, and a Z-pinch load. The Marx generator consists of sixteen 0.66-μF capacitors charged in parallel to a voltage of 75 kV and then discharged in series to the PFL. The PFL uses deionized water as insulating dielectric and is 1.67 m long, forming a pulse of 100 ns. The characteristic impedance of the PFL is 1.25 Ω. The parameters of the PTL are the same as those of the PFL.

The experimental arrangement for backlighting of the wire-array Z-pinch using two X-pinches as the x-ray sources is shown in Fig. 6. The wire-array Z-pinch as the imaged target was connected between the anode and the cathode. The two X-pinches as the x-ray sources in parallel were placed between the anode and the current return cylinder. The discharge current flowed through the wire-array Z-pinch from cathode to anode, and then returned via the two parallel X-pinches to the current return cylinder. The current was measured with a Rogowski coil. The x-rays emitted from the two X-pinches

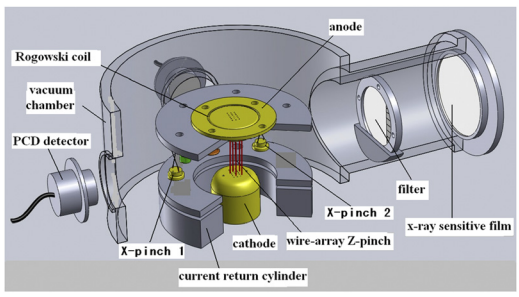

FIG. 6. Experimental arrangement for x-ray backlighting of wire-array Z-pinch.

passed through the wire-array Z-pinch plasma as well as the visible-light filter and arrived at the x-ray-sensitive film. Thereby, x-ray backlighting images of the EEWA were obtained. To determine the time at which the image was taken, the x-ray pulses from the two X-pinches were recorded with a photoconducting detector (PCD).

Figure 7 shows typical images of EEWA in which two molybdenum wires of diameter 50 μm spaced 2 mm apart were electrically exploded. According to the x-ray pulses from the two X-pinches [Fig. 3(c)], we know that two images were taken at times of 61 ns and 67 ns, at which the currents flowing through the wire-array Z-pinch were 172 kA and 188 kA, respectively.

From Figs. 7(a) and 7(b), it can be seen that EEWA usually exhibits a core–corona structure, i.e., a dense wire core surrounded by a corona plasma of low density, instead of one in which the wires are completely vaporized.[10] The corona plasma of each wire takes the shape of a "bamboo joint," similar to an $m = 0$ plasma instability. Furthermore, under the influence of the global magnetic field produced by the wire-array current, the highly conducting corona plasma first arrives at the axis of the wire array and forms a precursor plasma that exhibits high-order ($m > 0$) plasma instabilities. The core–corona structure and its inducing precursor plasma are both detrimental to the Z-pinch. In addition to inducing plasma instabilities, the core–corona structure prevents the plasma implosion from being simultaneous, with the dense core reaching the axis significantly later than the precursor plasma.

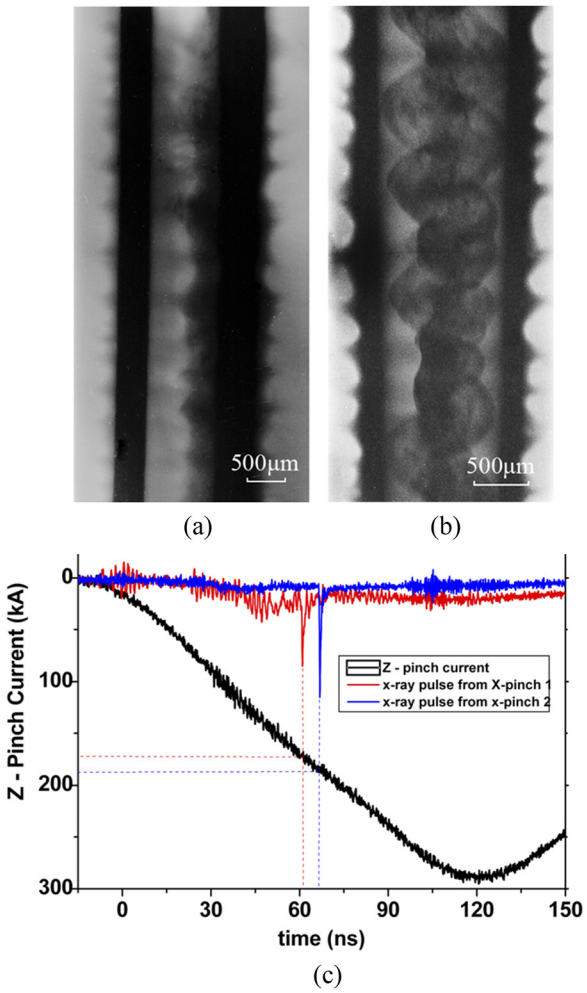

FIG. 7. Typical images of EEWA with two molybdenum wires of diameter 50 μm spaced 2 mm apart: (a) 61 ns, 172 kA; (b) 67 ns, 188 kA. (c) Waveforms of the current and x-ray pulses.

Much effort has been expended on suppressing the formation of a core–corona structure.[11–14] We believe that the main reason for the formation of this structure is as follows. During EEWA, the electron emission from the wire surfaces triggers an early flashover along these surfaces, as a result of which most of the current is transferred from the highly resistive wire core to the highly conducting corona plasma, and further energy deposition into the residual core almost comes to a halt. Therefore, if we could delay the flashover as much as possible, we might be able to suppress formation of the core–corona structure and realize a core-free EEW, with the whole wire uniformly vaporizing and then completely exploding into plasma.

A method for realizing core-free EEW has indeed been found, by inserting an insulator as a flashover switch into the cathode, as shown in Fig. 8. Only a single wire is used.

The flashover switch has two favorable effects on EEW. First, it steepens the voltage pulse applied to the wire and makes flashover along the wire surface more difficult. Second, it raises the electric potential of the wire relative to the cathode, because there is still a potential drop across the insulator in the process of surface flashover over the insulator, which causes the radial electric field on the wire surface to change from negative to positive in the case where a negative pulsed voltage is applied to the cathode and the anode is grounded. Here, a

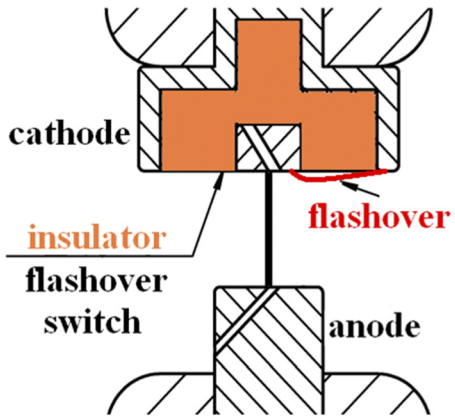

FIG. 8. An insulator as a flashover switch inserted in the cathode to realize core-free EEW.

positive radial field is defined as one in which the direction of the field is outward from the wire surface.[15]

The radial fields on the wire surface at the time at which wire melting begins were calculated with electrostatic simulation using COMSOL software. The results are shown in Fig. 9. When the radial field is positive, it depresses the surface electron emission that triggers early flashover along the wire surface.

The validity of the method was verified by calculation of the deposition energy before the flashover along the wire surface and by taking interferograms of EEWs with and without the flashover switch. Here, we take as an example EEW of a tungsten wire of length 1 cm and diameter 12.5 μm. For tungsten, the deposition energy required for the whole wire to completely vaporize is 8.8 eV/atom; i.e., the vaporization energy E_v for tungsten is 8.8 eV/atom.

The deposition energy can be calculated as follows:

$$E_d(t) = \int_0^{T_f} u_R(t) \cdot i(t) \cdot dt = \int_0^{T_f} \left[u_w(t) - L_w \frac{di(t)}{dt} \right] \cdot i(t) \cdot dt, \quad (1)$$

where u_R is the resistive voltage of the wire, i and u_w are the measured wire current and voltage, respectively, L_w is the calculated wire inductance, and T_f is the time instant at which flashover along the wire surface occurs.

For EEW without the flashover switch, the deposition energy is only 3.4 eV/atom and is thus significantly lower than E_v. Correspondingly, a dense core is visible in the center of the interferogram, as shown in Fig. 10(a). In contrast, for EEW with the flashover switch, the deposition energy rises to 12 eV/atom, which is higher than E_v. No residual core can be seen in the interferogram, which confirms the realization of core-free EEW.

In summary, then, we have developed a new method of inserting a flashover switch into the cathode to realize core-free EEW of a single wire in vacuum. Although the flashover switch can also be considered as a peaking switch, the effect of which in steepening a voltage pulse is well known, a second effect of this flashover switch in changing the radial field of the wire surface from negative to positive has been reported here for the first time. This second effect reduces the electron emission from the wire surface, which plays a more important role in realizing a core-free EEW. We are now applying this method to wire arrays and hope that it will similarly be successful in realizing core-free EEWA.

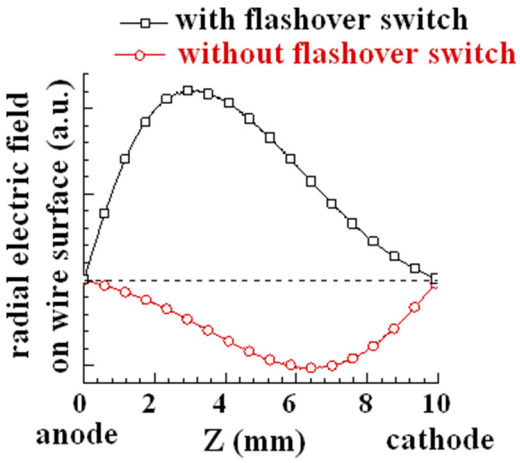

FIG. 9. Radial electric fields on the wire surface.

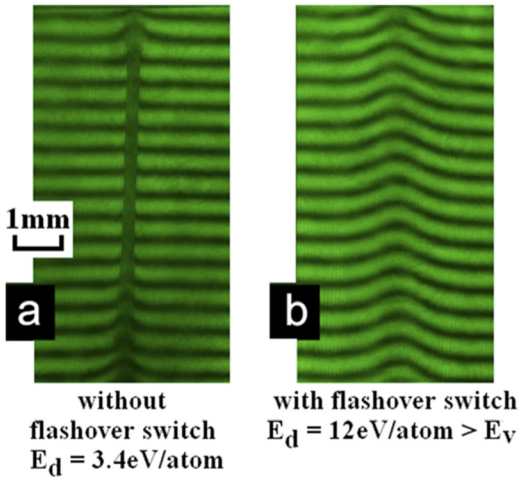

FIG. 10. Interferograms of EEW (a) without and (b) with a flashover switch.

III. EEW IN GASES FOR NANOPOWDER PRODUCTION

When EEW is performed in a gas at pressures from 0.1 to 1 atm, the metallic vapor is cooled by collisions with gas molecules, with nanoparticles being formed from the condensed vapor.[16–18] EEW of different wires in different gases can be used to produce different nanopowders, including metallic nanopowders, metallic oxide nanopowders, metallic nitride nanopowders, metallic carbide nanopowders, and carbon nanomaterials.

Figure 11 shows the experimental setup. It consists of eight 0.25-μF capacitors in parallel for energy storage, a gas spark-gap

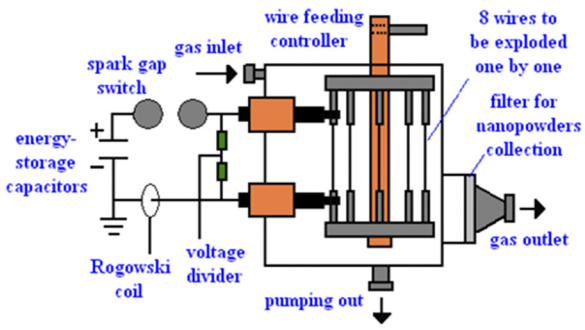

FIG. 11. Experimental setup of EEW for nanopowder production.

switch, and a discharge chamber housing eight wires to be exploded one by one. The experiment was performed according to the following procedure. The eight wires were installed in the discharge chamber, from which the existing gas was pumped out, to be replaced by the working gas. The capacitors were then charged to the working voltage. When the spark-gap switch was triggered, a pulsed current flowed through whichever of the eight wires was connected to the circuit, causing it to explode with the formation of nanopowder. The wires were exploded one by one in sequence as the wire feeding controller was turned. Finally, the working gas was pumped out and the discharge chamber was opened to allow collection of the nanopowder accumulated on the filter covering the gas outlet.

We investigated how different experimental conditions affect nanoparticle size by changing the wire (material and diameter), the gas (gas type and pressure), and the charging voltage of the energy-storage capacitors.[19] Here, we take as an example EEW of titanium wires in nitrogen for the production of metallic nitride nanopowders. The titanium wires were 85 mm in length and 0.23 mm in diameter. The charging voltage was changed in the range from 9 kV to 24 kV, causing the discharge current to rise from 6 kA to 25 kA.

As can be seen from the results in Fig. 12, which were obtained when the nitrogen pressure was kept at 20 kPa, both the deposition rate η and the plasma energy W_p increased with the charging voltage along with the discharge current, where the deposition rate is defined as the ratio E_d/E_v and the plasma energy as the energy deposited in the plasma produced by the breakdown of the metallic vapor. Figure 13 shows typical transmission electron microscope (TEM) images of the nanoparticles.

The specific surface area S of the nanoparticles was measured using the Brunauer–Emmett–Teller (BET) method of multilayer gas absorption. The average diameter of the nanoparticles was calculated from

$$d = \frac{6\times10^3}{\rho S} \quad [\mathrm{nm}], \tag{2}$$

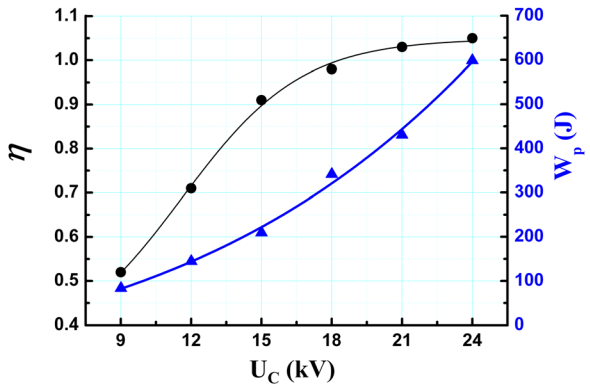

FIG. 12. Dependences of deposition rate η and plasma energy W_p on charging voltage.

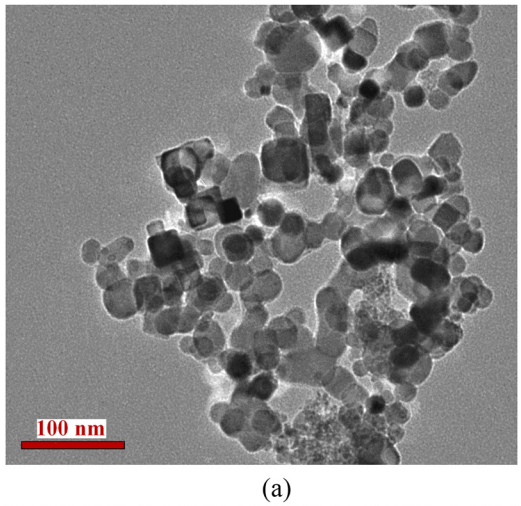

(a)

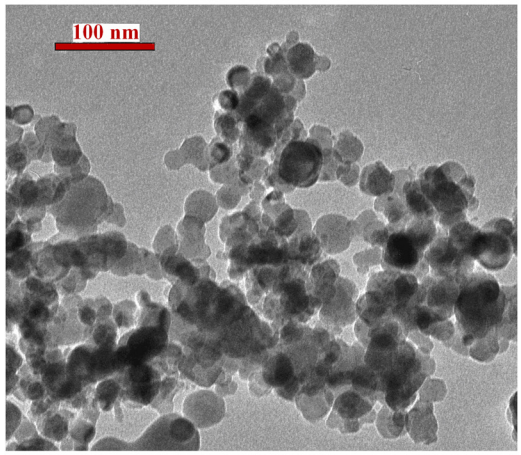

(b)

FIG. 13. TEM images of nanopowders obtained with charging voltages of (a) 9 kV and (b) 24 kV.

where ρ is the density of the nanoparticles. Figure 14 shows the results.

The dependence of nanoparticle size on nitrogen pressure was also investigated, with the charging voltage being kept at 18 kV. Figure 15 presents the results.

It was found that there are three parameters that determine the size of the nanoparticles produced by EEW. The first parameter is the deposition ratio. A higher η favors complete vaporization of the wire, without any residual liquid drops, which is good for obtaining smaller nanoparticles. The second parameter is the gas pressure. A lower pressure is favors faster vapor expansion and cooling, leading to smaller nanoparticles. The final parameter is the plasma energy. A lower W_p will not heat the surrounding gas to a high temperature, and thus will favor faster vapor cooling and smaller nanoparticles.

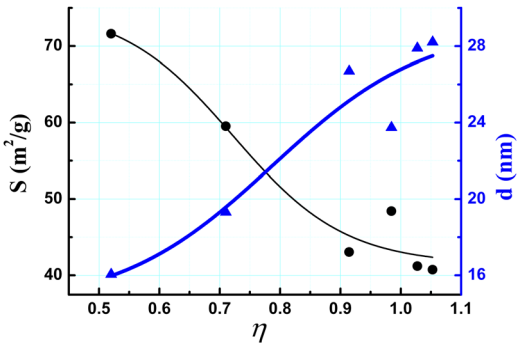

FIG. 14. Dependences of specific surface area and average diameter of nanoparticles on deposition rate η at a nitrogen pressure of 20 kPa.

In summary, EEW in different gases is an easy way to get different nanopowders. However, there are two improvements that need to be made before this method can move to industrial application. First, there must be greater uniformity in nanoparticle size. Second, the method must be adapted to allow automatic and continuous wire feeding.

IV. EEW IN LIQUID FOR SHOCK-WAVE GENERATION

When EEW is performed in a liquid, shock waves are generated by the rapid volume expansions accompanied by fast phase transitions.[1,20] EEW in a liquid is an efficient method for generating shock waves. For a spherical wire array of diameter 20 mm and made of 35 wires each of diameter 0.12 mm, a shock wave of 6 TPa at the center of the sphere can be expected with only a moderate current of 300 kA in amplitude and 1.1 μs in rise time.[21,22] Shock waves generated by EEW in liquid have a growing number of applications,[23] such as increasing production and enhancing recovery in oil wells, target ignition in inertial confinement fusion, and driving phase transitions in warm dense matter. We conducted two experiments on EEW in water. The first was an underheat experiment in which the deposition energy was lower than the vaporization energy, while the second focused on the effect of the current rise rate on the EEW for a given storage energy in the capacitors.

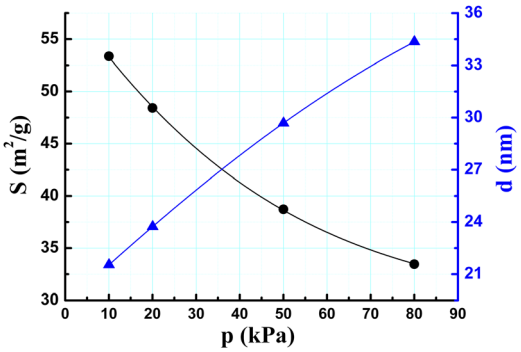

FIG. 15. Dependences of specific surface area and average diameter of nanoparticles on nitrogen pressure at a charging voltage of 80 kV.

A. Underheat experiment

EEW was performed in a water chamber of diameter 560 mm and height 500 mm. The copper wire to be exploded was immersed in the water inside the chamber. A 1-μF energy-storage capacitor was placed inside an oil tank outside the water chamber. In the underheat experiment, the energy-storage capacitor was charged to a relatively low energy so that the energy deposited into the wire was not large enough to completely vaporize the wire. Through a field distortion switch and a high-voltage cable outside the water chamber, the energy-storage capacitor discharged to the wire inside the water chamber. The waveforms of the discharge current i(t) and the wire voltage u(t) were directly measured with a Pearson 101 Rogowski coil (with a bandwidth of 4 MHz) and a Tektronix P6015A voltage divider (with a bandwidth of 75 MHz), respectively. A Piezotronics PCB138 pressure probe was placed 100 mm away from the wire and used to record the waveform of the shock wave.

It was found that the shock waves had poor reproducibility owing to only partial vaporization of the exploding wire. Although a partial vaporization rate as low as 6% is enough to generate a shock wave, the amplitude of the latter depends strongly on the vaporized mass of the wire. The greater the vaporized mass, the stronger is the shock wave.[24]

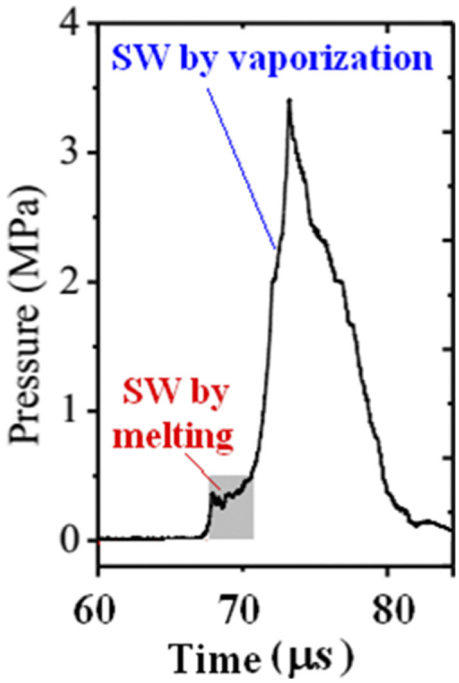

FIG. 16. Typical shock-wave pressure waveform showing two shock waves (SW): one generated by melting and the other by vaporization.

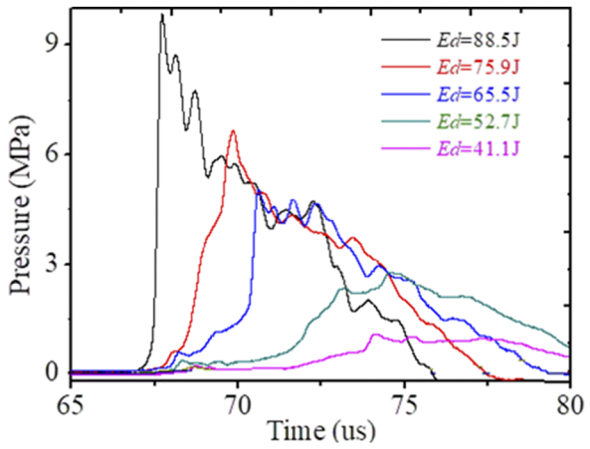

FIG. 17. Process by which the shock wave generated by vaporization overtakes the shock wave generated by melting as E_d increases.

It is widely accepted that the generation of shock waves by EEW in water is due to rapid volume expansion accompanied by phase transitions, such as melting of solid, vaporization of liquid, and formation of plasma. In the past, the formation of shock waves by wire melting could only be observed using expensive streak cameras that are not available in most laboratories. The reason why shock waves generated by melting have never been observed with commonly used piezoelectric gauges is as follows. To avoid damage by the wire explosion, a piezoelectric gauge must be placed some distance from the wire. By the time it has reached such a distance, a shock wave generated by melting will have been overtaken by and immersed within the stronger and faster shock wave generated by vaporization and therefore will not be detected by the piezoelectric gauge. However, it was found that in an underheat experiment, the partial vaporization generates a significantly weaker and slower shock wave that is unable to overtake the shock wave generated by melting, and the latter can therefore be detected by a piezoelectric gauge. Figure 16 shows a typical waveform of shock-wave pressure recorded by a piezoelectric gauge located 100 mm from an exploding copper wire of length 50 mm and diameter 0.2 mm. The deposition energy was 57 J, while the complete vaporization energy for this copper wire was 86 J. In Fig. 16, there is a prepulse in the form of a small plateau, followed by a main pulse. The prepulse was identified with the shock wave generated by melting and the main pulse with the shock wave generated by vaporization.

The pressure–time curves in Fig. 17 show clearly the process in which the shock wave generated by vaporization overtakes the shock wave generated by melting.[25] As the deposition energy is gradually raised from 41.1 J to 88.5 J and the EEW changes from an underheat EEW to a overheat EEW, the main pulse representing the shock wave generated by vaporization becomes stronger and faster. As a result, the main pulse approaches closer and closer to the prepulse representing the shock wave generated by melting. Finally, when the deposition energy reaches 88.5 J, the shock wave generated by vaporization overtakes the shock wave generated by melting, and the latter can no longer be observed. The pressure–time curve then takes the form obtained in most previous experiments in which as much energy as possible was deposited into the wire in order to generate the strongest possible shock wave.

B. EEW at a given storage energy for two different capacitor banks

In the experiment to investigate the effect of the current rise rate on EEW, the experimental setup was almost the same as that used in the underheat experiment. Two capacitor banks of 1 μF and 200 μF were used. They were charged to different voltages for the same storage energy in the range from 70 J to 1.8 kJ. In this case, the rise rate of the current using the small capacitor bank of 1 μF was much greater than that using the large capacitor bank of 200 μF. It was found that the resulting EEWs were significantly different. Here we take as an example the EEW of a copper wire using the two capacitor banks, each charged to an energy of 121 J. The copper wire was 0.12 mm in diameter and 50 mm in length, corresponding to a complete vaporization energy of 31 J. A comparison of the parameters for EEW using these two capacitor banks is given in Table I.

The discharge mode of EEW was the cutoff current mode when the 200-μF capacitor bank was used, but the restrike mode when the 1-μF bank was used, as shown in Fig. 18. The rise rate of the current when the 1-μF bank was used was about 10 times that with the 200-μF bank. Consequently, an overheat EEW using the 1-μF bank produces a shock wave about 21 times stronger than that produced by underheat EEW using the 200-μF bank.

TABLE I. Comparison of parameters for EEW using two capacitor banks.

	200-μF capacitor bank	200-μF capacitor bank
Discharge mode	Cutoff current	Restrike
Current peak (kA)	2.4	6.7
Voltage peak	2.2	45
di/dt (kA/μs)	0.68	7.50
Deposition energy (J)	10.1	40.8
EEW mode	Underheat	Overheat
Shock-wave pressure (MPa)	0.53	11.58

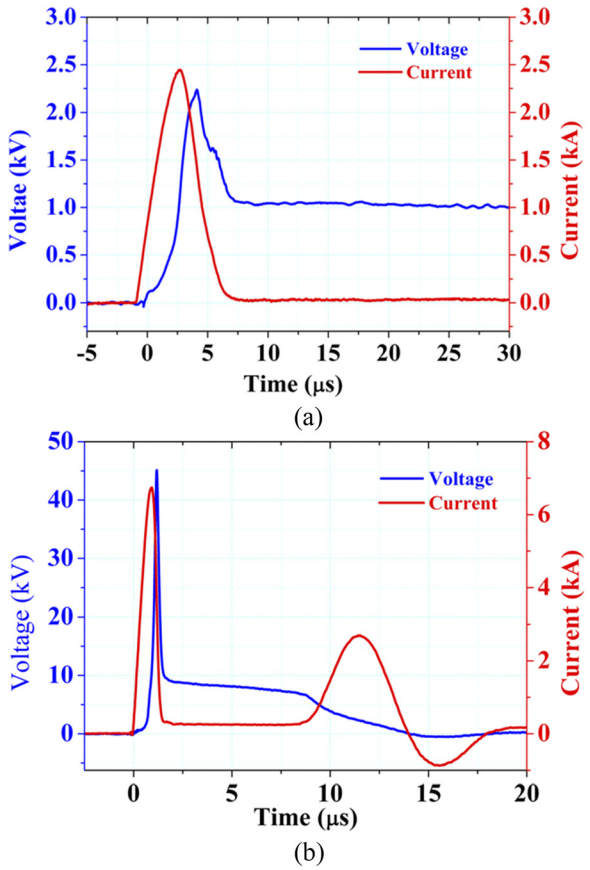

FIG. 18. Comparison of discharge modes: (a) cutoff current mode with the 200-μF capacitor bank; (b) restrike mode with the 1-μF capacitor bank.

In summary, in previous work, the focus has usually been on experiments with overheat, in order to produce as strong as possible a shock wave. In our underheat experiment, we hoped to find new phenomena and investigate the underlying physics. In this experiment, we observed a phenomenon in which the shock wave generated by vaporization overtook the shock wave generated by melting. By comparing the results of an overheat experiment using a 1-μF capacitor bank with those of an underheat experiment using a 200-μF bank, we found significant differences in the rise rates of the current and in the discharge modes, leading to a great difference in the amplitudes of the shock waves generated. We are now trying to use shock waves generated by this technique to increase production and enhance recovery in oil wells.

V. CONCLUSIONS

EEW in vacuum was used to produce an X-pinch that proved to be an ideal point x-ray source for phase-contrast imaging of weakly x-ray absorbing samples such as small insects like mosquitoes and ants. The images show clearly the internal structures of these samples, which cannot be seen with conventional x-ray radiography, indicating the potential biological and clinical applications of this technique. We are now examining the possibility of using this technique in mammography, in which there is a need to distinguish between different kinds of soft tissue, namely, tumors and normal tissue. Because the absorption is small, and the differences in density and composition are slight, conventional x-ray radiography is not very successful at this task.

EEW in vacuum was used to produce a wire-array Z-pinch. Electrical explosion of a wire array (EEWA) often exhibits a core–corona structure that is detrimental to the plasma implosion of a Z-pinch. By inserting an insulator as a flashover switch into a negatively biased cathode, the formation of the core–corona structure was suppressed and a core-free EEWA was realized. Although the flashover switch can also be considered as a peaking switch, with a well-known effect in steepening the voltage pulse, a second effect of this flashover switch in changing the radial field of the wire surface from negative to positive was reported here for the first time. This second effect suppresses electron emission from the wire surface and thereby plays a more important role in realizing a core-free EEW. We are now applying this method to wire arrays in the hope that it will be similarly successful in realizing core-free EEWA.

EEW in gases was used for nanopowder production. Three parameters (vaporization rate, gas pressure, and energy deposited in the exploding plasma) were found to influence the nanoparticle size. Although EEW in different gases is an easy route for the production of different nanopowders, there are two obstacles to be overcome before this method can be applied in industry: the uniformity of nanoparticle size needs to be improved, and techniques for automatic and continuous wire feeding need to be developed.

In previous studies of the generation of shock waves by EEW in liquids, the focus was usually on experiments with overheat, in order to obtain shock waves that were as strong as possible. The aim of our underheat experiment, in contrast, was to discover new phenomena and the underlying physics. We observed a phenomenon in which the shock wave generated by vaporization overtook the shock wave generated by melting. By comparing the results of an overheat experiment using a 1-μF capacitor bank with those of an underheat experiment using a 200-μF bank, we found significant differences in the rise rates of the current and in the discharge modes, leading to a great difference in the amplitudes of the shock waves generated.

ACKNOWLEDGMENTS

The author would like to thank all the colleagues and students who have made contributions to the research on EEW at Tsinghua University. The author would also like to thank the National Natural Science Foundation of China for supporting this work under Contract Nos. 50677034, 10635050, 51237006, and 51777113.

REFERENCES

[1]W. G. Chance and H. K. Moore, Exploding Wires (Plenum Press, 1962).
[2]S. A. Pikuz, T. A. Shelkovenko, and D. A. Hammer, "X-pinch. Part 1," Plasma Phys. Rep. **41**, 291 (2015).
[3]S. W. Wilkins, T. E. Gureyev, D. Gao, A. Pogany, and A. W. Stevenson, "Phase-contrast imaging using polychromatic hard x-rays," Nature **384**, 335 (1996).
[4]R. Fitzgerald, "Phase-sensitive x-ray imaging," Phys. Today **53**(7), 23 (2000).
[5]R. Liu, X. X. Wang, X. B. Zou, N. G. Zeng, and L. Y. He, "Phase-contrast imaging of a soft biological object using x-pinch as x-ray source," Europhys. Lett. **83**, 25002 (2008).
[6]H. G. Haines, "A review of the dense Z-pinch," Plasma Phys. Control. Fusion **53**, 093001 (2011).
[7]C. Deeney, M. R. Douglas, R. B. Spielman, T. J. Nash, D. L. Peterson *et al.*, "Enhancement of x-ray power from a Z pinch using nested-wire arrays," Phys. Rev. Lett. **81**, 4883 (1998).
[8]T. Zhao, X. Zou, R. Zhang, and X. Wang, "X-ray backlighting of two-wire Z-pinch plasma using X-pinch," Chin. Phys. B **19**, 075205 (2010).
[9]X. Zou, R. Liu, N. Zeng, M. Han, J. Yuan *et al.*, "Pulsed power generator for X-pinch," Laser Part. Beams **24**, 503 (2006).
[10]S. V. Lebedev, F. N. Beg, S. N. Bland, J. P. Chittenden, A. E. Dangor *et al.*, "Effect of discrete wires on the implosion dynamics of wire array Z pinches," Phys. Plasmas **8**, 3734 (2001).
[11]A. J. Harvey-Thompson, S. V. Lebedev, G. Burdiak, E. M. Waisman, G. N. Hall *et al.*, "Suppression of the ablation phase in wire array Z pinches using a tailored current prepulse," Phys. Rev. Lett. **106**, 205002 (2011).
[12]G. S. Sarkisov, S. E. Rosenthal, K. W. Struve, and D. H. McDaniel, "Corona-free electrical explosion of polyimide-coated tungsten wire in vacuum," Phys. Rev. Lett. **94**, 035004 (2005).
[13]E. V. Grabovskii, A. N. Gribov, K. N. Mitrofanov, G. M. Oleinik, I. Yu. Porofeev *et al.*, "Influence of the current growth rate on the polarity effect in a wire array in the angara-5-1 facility," Plasma Phys. Rep. **33**, 923 (2007).
[14]G. S. Sarkisov, S. E. Rosenthal, K. W. Struve, T. E. Cowan, R. Presura *et al.*, "Effect of current prepulse on wire array initiation on the 1-MA ZEBRA accelerator," Phys. Plasmas **14**, 052704 (2007).
[15]H. Shi, X. Zou, and X. Wang, "Fully vaporized electrical explosion of bare tungsten wire in vacuum," Appl. Phys. Lett. **109**, 134105 (2016).
[16]Y. A. Kotov, "Electric explosion of wires as a method for preparation of nanopowders," J. Nanopart. Res. **5**, 539 (2003).
[17]W. H. Jiang and K. Yatsui, "Pulsed wire discharge for nanosize powder synthesis," IEEE Trans. Plasma Sci. **26**, 1498 (1998).
[18]C. H. Cho, S. H. Park, Y. W. Choi *et al.*, "Production of nanopowders by wire explosion in liquid media," Surf. Coat. Technol. **201**, 4847 (2007).
[19]X. B. Zou, Z. G. Mao, X. X. Wang, and W. H. Jiang, "Two different modes of wire explosion for nanopowder production," Europhys. Lett. **97**, 35004 (2012).
[20]Ya. E. Krasik, A. Fedotov, D. Sheftman, S. Efimov, A. Sayapin *et al.*, "Underwater electrical wire explosion," Plasma Sources Sci. Technol. **19**, 034020 (2010).
[21]O. Antonov, S. Efimov, D. Yanuka, M. Kozlov, V. Tz. Gurovich, and Ya. E. Krasik, "Generation of converging strong shock wave formed by microsecond timescale underwater electrical explosion of spherical wire array," Appl. Phys. Lett. **102**, 124104 (2013).
[22]Ya. E. Krasik, S. Efimov, D. Sheftman, A. Fedotov, O. Antonov *et al.*, "Underwater electrical explosion of wire and wire arrays and generation of converging shock waves," IEEE Trans. Plasma Sci. **44**, 412 (2016).
[23]Ya. E. Krasik, A. Grinenko, A. Sayapin, S. Efimov, A. Fedotov *et al.*, "Underwater electrical wire explosion and its applications," IEEE Trans. Plasma Sci. **36**, 423 (2008).
[24]L. Li, D. Qian, X. Zou, and X. Wang, "Effect of deposition energy on underwater electrical wire explosion," IEEE Trans. Plasma Sci. **46**, 3444 (2018).
[25]L. Li, D. Qian, X. Zou, and X. Wang, "Underwater electrical wire explosion: Shock wave from melting being overtaken by shock wave from vaporization," Phys. Plasmas **25**, 053502 (2018).